The effect of Dzyaloshinskii-Moriya interaction on field-driven domain wall dynamics analysed by a semi-analytical approach

The effect of the Dzyaloshinskii-Moriya interaction on field-driven domain wall dynamics analysed by a semi-analytical approach

J Vandermeulen[1,2], S A Nasseri[3,4], B Van de Wiele[1], G Durin[3,5], B Van Waeyenberge[2] and L Dupré[1]

E-mail: jasper.vandermeulen@ugent.be
[1] Department of Electrical Energy, Systems and Automation, Ghent University, B-9000 Ghent, Belgium.
[2] Department of Solid State Sciences, Ghent University, Krijgslaan 281-S1, B-9000 Ghent, Belgium.
[3] ISI Foundation, Via Alassio 11/c, 10126 Torino, Italy.
[4] Politecnico di Torino, Corso Duca degli Abruzzi 24, 10129 Torino, Italy.
[5] Istituto Nazionale di Ricerca Metrologica, Strada delle Cacce 91, 10135 Torino, Italy.

Abstract. Fast domain wall (DW) propagation through perpendicularly magnetized nanostrips with Dzyaloshinskii-Moriya interaction (DMI) offers promising opportunities for the development of magnetic memory and logic devices. However, as the DW speed increases, the DW magnetization is also progressively affected which ultimately leads to an unstable DW and a drop in the velocity, i.e. the Walker breakdown. In this paper, we introduce a semi-analytical approach to describe and quantify changes to the internal degrees of freedom of the DW. By spatially averaging the Landau-Lifshitz-Gilbert equation, we derive equations of motion and identify seven DW variables in addition to the DW position. This contrasts analytical models where such variables are introduced in an ansatz for the DW shape. We apply this to field driven DW motion and study the effect of DMI in detail. Our method helps characterize the opposing and reinforcing effects of the different interactions involved, contributing to our understanding of the Walker breakdown.

PACS numbers: 71.70.Gm, 75.60.Ch, 75.78.Fg, 75.78.Cd

Keywords magnetic domain wall motion, magnetic nanostrips, Dzyaloshinskii-Moriya interaction, PMA, micromagnetics

Submitted to: *J. Phys. D: Appl. Phys.*

Accepted: J. Phys. D: Appl. Phys. 49 (2016) 465003 (13pp).
DOI: *10.1088/0022-3727/49/46/465003*

1. Introduction

Nowadays, much research is devoted towards the understanding and improvement of magnetic domain wall (DW) motion in magnetic nanostrips to aid in the development of promising non-volatile logic and memory devices [1]. While most concepts use magnetic domains to represent the digital data [2–5], alternative concepts based on magnetic DWs have recently been proposed [6, 7].

In multilayered out-of-plane magnetized nanostrips, the interfacial Dzyaloshinskii-Moriya interaction (DMI) [8, 9] can significantly enhance DW mobility. Therefore, the effect of DMI on DW motion has been thoroughly investigated experimentally, computationally and theoretically [10–17]. Recently, the widely used one dimensional (1D) analytical model describing DW dynamics through a nanostrip [18–20] was extended to account for the effect of the DMI on DWs [10, 11]. The equations of motion in these analytical models are derived using a Lagrangian approach based on an ansatz describing the DW shape as a rigid structure. While conventional analytical models ($q-\phi$ or $q-\phi-\Delta$) describe DW motion in nanostrips by two or three collective coordinates [21, 22] – the DW position q, the magnetization angle ϕ [18] and the DW width Δ when three collective coordinates are considered [10] – an extra collective coordinate χ, representing the tilting angle of the DW plane, was introduced in the ansatz [11].

While analytical models have the advantage that they are predictive and no micromagnetic simulations are needed to interpret the equations of motion, they are not always very precise in predicting DW dynamics [11, 15]. Therefore, in this paper, a semi-analytical approach is used in accordance with micromagnetic simulations, taking changes to the internal degrees of freedom of the DW into account without an ansatz for the DW profile. Earlier versions of this approach were already able to succesfully describe DW dynamics in in-plane magnetized and PMA nanostrips, taking into account effects due to finite temperature and disorder [23–25].

To investigate the DMI in detail, we use the semi-analytical approach on field-driven DW dynamics. First, we determine an expression for the DW position. Subsequently, the Landau-Lifshitz-Gilbert equation is spatially averaged, resulting in equations of motion with variables describing the DW. Next to the DW position, seven variables are identified.

The equations of motion clearly show how the internal effective fields add up to balance the driving out-of-plane field. To quantify these contributions, we have used micromagnetic simulations. Their opposing/reinforcing effect is then investigated for varying out-of-plane fields and several in-plane fields to gain more insight. An accompanying interpretation is given based on the variables. Finally, we also investigate and interpret the relative importance of these interactions at the Walker breakdown (WB) as a function of varying DMI strengths. It helps us understand the changes to the internal degrees of freedom of the DW and their effect on shifting the WB to higher/lower driving fields.

2. The equations of motion

Magnetization dynamics is governed by the Landau-Lifshitz-Gilbert equation

$$\frac{\partial \mathbf{m}}{\partial t}(\mathbf{r},t) = \frac{\gamma_0}{1+\alpha^2}(\mathbf{H}_{\text{eff}}(\mathbf{r},t) \times \mathbf{m}(\mathbf{r},t))$$

$$+\frac{\alpha\gamma_0}{1+\alpha^2}\mathbf{m}(\mathbf{r},t)\times(\mathbf{H}_{\text{eff}}(\mathbf{r},t)\times\mathbf{m}(\mathbf{r},t)) \tag{1}$$

with the magnetization represented as a continuum vector field with fixed magnitude $|\mathbf{m}(\mathbf{r},t)| = 1$ and variable orientation. In a multilayered out-of-plane magnetized nanostrip made of a heavy metal layer with strong spin orbit coupling and broken inversion symmetry, the interfacial Dzyaloshinskii-Moriya interaction (DMI) affects the magnetization dynamics. This is taken into account by the effective field

$$\begin{aligned}\mathbf{H}_{\text{eff}}(\mathbf{r},t) &= \mathbf{H}_{\text{ext}}+\mathbf{H}_{\text{ani}}+\mathbf{H}_{\text{ms}}+\mathbf{H}_{\text{DMI}}+\mathbf{H}_{\text{exch}}\\ &= \overbrace{\sum_{i=1}^{3}H_{\text{ext},i}\mathbf{e}_i}^{\text{external field}}+\overbrace{\frac{2K_{\text{u}}}{\mu_0 M_{\text{s}}^2}M_{\text{s}}m_z\mathbf{e}_z}^{\text{uniaxial anisotropy}}\overbrace{-\hat{N}\cdot M_{\text{s}}\mathbf{m}}^{\text{magnetostatic interaction}}\\ &\quad+\overbrace{\frac{2D_{\text{DMI}}}{\mu_0 M_{\text{s}}}\left[\nabla m_z-(\nabla\cdot\mathbf{m})\,\mathbf{e}_z\right]}^{\text{DMI}}\\ &\quad+\overbrace{\frac{2A}{\mu_0 M_{\text{s}}}\sum_{i=1}^{3}\nabla^2 m_i\mathbf{e}_i}^{\text{exchange interaction}}.\end{aligned} \tag{2}$$

Here, $\gamma_0 = \mu_0|\gamma|$ with γ the gyromagnetic ratio and μ_0 the permeability of vacuum, α the Gilbert damping constant [26] and M_{s} the saturation magnetization. The externally applied field $\mathbf{H}_{\text{ext}}$, anisotropy field $\mathbf{H}_{\text{ani}}$, magnetostatic field $\mathbf{H}_{\text{ms}}$, DMI-field $\mathbf{H}_{\text{DMI}}$ and exchange field $\mathbf{H}_{\text{exch}}$ contribute to the effective field $\mathbf{H}_{\text{eff}}$. In the micromagnetic simulations, the Landau-Lifshitz-Gilbert equation is solved in each finite difference cell. As the magnetization varies in space and time, this microscopic equation has a huge number of degrees of freedom which can be reduced in terms of a limited number of variables. In our semi-analytical approach, we quantify these variables from micromagnetic simulations.

Using a similar approach as in [23], we derive the equations of motion for a DW in a perpendicularly magnetized nanostrip driven by an out-of-plane field. In perpendicularly magnetized nanostrips without DMI and in-plane fields, the domain magnetization has no in-plane magnetized contributions as depicted in Figure 1(a). The DW position Q is then expressed as [27]

$$Q(t) = \frac{L_x}{2}\langle m_z(\mathbf{r},t)\rangle \tag{3}$$

with the average $\langle f\rangle$ taken over any volume of the nanostrip including the DW [23–25]. Considering that the DMI induces edge effects in the domains and in-plane fields cant the domain magnetization into the plane as depicted in Figure 1(b-d), eq. (3) is replaced by ($\partial_x = \frac{\partial}{\partial x}$)

$$Q(t) = \frac{1}{-\langle\partial_x m_z(\mathbf{r},t)\rangle}\langle m_z(\mathbf{r},t)\rangle. \tag{4}$$

So, we derive the DW velocity

$$v(t) \equiv \frac{\mathrm{d}Q(t)}{\mathrm{d}t}. \tag{5}$$

Restricting the averages $\langle f\rangle$ to the DW volume as detailed in Appendix A, we derive that

$$v(t) = \frac{1}{-\langle\partial_x m_z(\mathbf{r},t)\rangle}\frac{\mathrm{d}\langle m_z(\mathbf{r},t)\rangle}{\mathrm{dt}}. \tag{6}$$

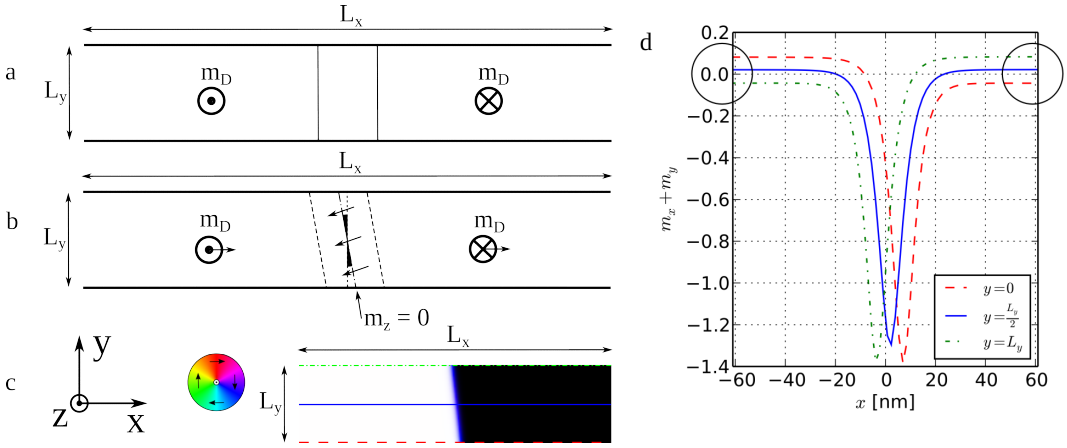

Figure 1. Sketch of a magnetic DW in an out-of-plane magnetized nanostrip with cross sectional dimensions $L_y \times L_z$ and length L_x (a) without DMI and in-plane fields and (b) with DMI and in-plane fields. In (c), a simulation snapshot of the situation in (b) is depicted with $D_{\mathrm{DMI}} = 0.4$ mJ/m^2, $\mu_0 H_{\mathrm{ext},x} = 20$ mT, $\mu_0 H_{\mathrm{ext},z} = 15$ mT, $L_x = 400$ nm, $L_y = 100$ nm and $L_z = 0.6$ nm. In (d), the corresponding $m_x + m_y$-values are plotted along the bottom ($y = 0$), middle ($y = L_y/2$) and top ($y = L_y$) of the nanostrip as a function of x. In situation (a), the left [right] domain has a magnetization in the positive [negative] z-direction while in situation (b,c), the magnetization of the domains is slightly tilted in the positive x-direction and edge effects are present, in agreement with (d) as highlighted by the black circles. Furthermore, the DW can also be geometrically tilted with respect to the y-direction (b,c,d). Averaged quantities $\langle f \rangle$ are obtained by averaging over the DW volume indicated by the dashed lines in (b). For more information regarding the calculation of these quantities and defining the averaging window, see Appendix A.

The analytical models demonstrate that, next to an equation for the DW velocity, an equation for the change in DW magnetization angle is necessary for describing DW dynamics [10, 11, 18–20]. Therefore, the in-plane magnetization angle $\phi(\mathbf{r}, t)$ is introduced

$$\phi(\mathbf{r}, t) = \arctan \frac{m_y(\mathbf{r}, t)}{m_x(\mathbf{r}, t)}. \tag{7}$$

For conciseness, we will not include the time and space dependency of variables in future equations.

In order to find the equations of motion for these coordinates, we average the LLG equation (1) over the DW. To this end, the *locally* varying effective field (2) is first properly averaged *over the DW volume*

$$\begin{aligned}
\mathbf{H}_{\mathrm{eff,DW}} &= \mathbf{H}_{\mathrm{ext}} + \left[\frac{1}{\zeta_{\mathrm{ani}}} \langle \mathbf{H}_{\mathrm{ani}} \rangle + \frac{1}{\zeta_{\mathrm{ms}}} \langle \mathbf{H}_{\mathrm{ms}} \rangle + \frac{1}{\zeta_{\mathrm{DMI}}} \langle \mathbf{H}_{\mathrm{DMI}} \rangle + \frac{1}{\zeta_{\mathrm{exch}}} \langle \mathbf{H}_{\mathrm{exch}} \rangle \right] \\
&\cong H_{\mathrm{ext},x} \mathbf{e}_x + H_{\mathrm{ext},y} \mathbf{e}_y + H_{\mathrm{ext},z} \mathbf{e}_z + \frac{2K_{\mathrm{u}}}{\mu_0 M_{\mathrm{s}} \zeta_{\mathrm{ani}}} \langle m_z \rangle \mathbf{e}_z \\
&- \frac{M_{\mathrm{s}}}{\zeta_{\mathrm{ms}}} \left[N_{\mathrm{eff},x} \langle m_x \rangle \mathbf{e}_x + N_{\mathrm{eff},y} \langle m_y \rangle \mathbf{e}_y + N_{\mathrm{eff},z} \langle m_z \rangle \mathbf{e}_z \right] \\
&+ \frac{2D_{\mathrm{DMI}}}{\mu_0 M_{\mathrm{s}} \zeta_{\mathrm{DMI}}} \left[\langle \partial_x m_z \rangle \mathbf{e}_x + \langle \partial_y m_z \rangle \mathbf{e}_y - \langle \partial_x m_x + \partial_y m_y \rangle \mathbf{e}_z \right]
\end{aligned}$$

$$+\frac{2A}{\mu_0 M_\mathrm{s}\zeta_\mathrm{exch}}\left[\langle\partial_{xx}m_x\rangle\mathbf{e}_x+\langle\partial_{yy}m_y\rangle\mathbf{e}_y+\langle\partial_{zz}m_z\rangle\mathbf{e}_z\right], \tag{8}$$

thereby introducing scaling factors ζ_ani, ζ_ms, ζ_DMI and ζ_exch. These scaling factors ensure that, while $\mathbf{H}_\mathrm{eff,DW}$ has a fixed value over the entire DW and $\mathbf{H}_\mathrm{eff}$ varies locally, they are physically equivalent when locally interacting with the DW magnetization from the perspective of the DW, i.e. after averaging these interactions over the entire DW. Note that due its uniformity, the external field $\mathbf{H}_\mathrm{ext}$ is not scaled.

If we assume that the DW is approximately a uniformly magnetized ellipsoid, the averaged magnetostatic field is approximated by an effective demagnetizing diagonal tensor $\hat{N}_\mathrm{eff}$ times the averaged magnetization

$$\langle\mathbf{H}_\mathrm{ms}\rangle\equiv-M_\mathrm{s}\langle N_{ij}(\mathbf{r},t)m_j(\mathbf{r},t)\rangle\cong-M_\mathrm{s}N_{\mathrm{eff},i}(t)\langle m_i\rangle(t)\ \forall i,j\in\{x,y,z\}. \tag{9}$$

where $\hat{N}$ is a local tensor [28]. This assumption is justified by the DW dimensions and the quasi uniformity of the in-plane magnetization direction [29]. Moreover, this simplifies the equations of motion and enables us to extract the effective demagnetizing factors from the micromagnetic simulations‡.

Subsequently, (6) and the temporal derivative of (7) are rewritten by explicitly evaluating and averaging equation (1) after inserting (8). This eventually leads to expressions for DW velocity and the change of magnetization in terms of DW variables. If we neglect the asymmetric terms in accordance with Appendix B, we derive following description for the DW velocity

$$\begin{aligned}\frac{-\langle\partial_x m_z\rangle}{\langle m_\mathrm{ip}^2\rangle}\frac{1+\alpha^2}{\gamma_0}v(\mathbf{H}_\mathrm{ext})=&\left[H_{\mathrm{ext},x}\frac{\langle m_y\rangle}{\langle m_\mathrm{ip}^2\rangle}-H_{\mathrm{ext},y}\frac{\langle m_x\rangle}{\langle m_\mathrm{ip}^2\rangle}+\alpha H_{\mathrm{ext},z}\right]\\&+M_\mathrm{s}(N_{\mathrm{eff},y}-N_{\mathrm{eff},x})\frac{\langle m_x\rangle\langle m_y\rangle}{\langle m_\mathrm{ip}^2\rangle\zeta_\mathrm{ms}}\\&+\frac{2D_\mathrm{DMI}}{\mu_0 M_\mathrm{s}}\left[\frac{\langle\partial_x m_z\rangle\langle m_y\rangle}{\langle m_\mathrm{ip}^2\rangle\zeta_\mathrm{DMI}}-\frac{\langle\partial_y m_z\rangle\langle m_x\rangle}{\langle m_\mathrm{ip}^2\rangle\zeta_\mathrm{DMI}}\right]\\&+\frac{2A}{\mu_0 M_\mathrm{s}}\left[\frac{\langle\partial_{xx}m_x\rangle\langle m_y\rangle}{\langle m_\mathrm{ip}^2\rangle\zeta_\mathrm{exch}}-\frac{\langle\partial_{yy}m_y\rangle\langle m_x\rangle}{\langle m_\mathrm{ip}^2\rangle\zeta_\mathrm{exch}}\right]\end{aligned} \tag{10}$$

with $\mathbf{m}_\mathrm{ip}$ a magnetization vector that only takes into account the in-plane magnetization

$$\mathbf{m}_\mathrm{ip}\equiv m_x\mathbf{e}_x+m_y\mathbf{e}_y. \tag{11}$$

From this equation, we immediately get that

$$\langle m_\mathrm{ip}^2\rangle=\langle m_x^2+m_y^2\rangle \tag{12}$$

and

$$\langle|m_\mathrm{ip}|\rangle\equiv\langle\sqrt{m_x^2+m_y^2}\rangle. \tag{13}$$

To determine the scaling factors in (10), we have to rewrite this equation to enable a comparison with the analytical 1D models [20]. In the analytical 1D models, q, ϕ

‡ The extraction of the effective demagnetizing factors from the micromagnetic simulations implies that even in cases where the assumption does not make any sense, the averaged magnetostatic field is still described within good accuracy.

and Δ represent respectively the DW position, the DW magnetization angle and the DW width. Analogously, we postulate the DW width Δ_{av} as

$$\Delta_{\mathrm{av}} \equiv 2\frac{\langle m_{\mathrm{ip}}^2\rangle}{-\langle \partial_x m_z\rangle} \tag{14}$$

with $\langle \partial_x m_z\rangle$ compensating for the averaging window as discussed in Appendix A. Without DMI and in-plane fields, eq. (14) is simplified to $\Delta_{\mathrm{av}} = L_x\langle m_{\mathrm{ip}}^2\rangle$ in agreement with our previous formulation [23–25]. Furthermore, we identify $\frac{\langle m_y\rangle}{\langle |m_{\mathrm{ip}}|\rangle}$ and $\frac{\langle m_x\rangle}{\langle |m_{\mathrm{ip}}|\rangle}$ as respectively the sine and cosine of an average magnetization angle Φ_{av}. Equivalently, we can write

$$\tan\Phi_{\mathrm{av}} = \frac{\langle m_y\rangle}{\langle m_x\rangle}, \tag{15}$$

an expression closely related to the definition of $\phi(\mathbf{r},t)$ (7). To define Φ_{av} unambiguously, we impose that $\Phi_{\mathrm{av}} = 0$ corresponds to a Néel wall characterized by $\langle m_y\rangle = 0$ and $\langle m_x\rangle > 0$ while $\Phi_{\mathrm{av}} = \pi$ corresponds to a Néel wall characterized by $\langle m_y\rangle = 0$ and $\langle m_x\rangle < 0$. If we restrict ourselves to field driven DW motion in a PMA nanostrip without DMI and in-plane fields, eq. (10) then simplifies to

$$\begin{aligned}\frac{2}{\Delta_{\mathrm{av}}}\frac{1+\alpha^2}{\gamma_0}v(\mathbf{H}_{\mathrm{ext}}) &= \alpha H_{\mathrm{ext},z} \\ &\quad + M_{\mathrm{s}}(N_{\mathrm{eff},y} - N_{\mathrm{eff},x})\frac{\langle |m_{\mathrm{ip}}|\rangle^2}{\langle m_{\mathrm{ip}}^2\rangle\zeta_{\mathrm{ms}}}\frac{\sin 2\Phi_{\mathrm{av}}}{2}\end{aligned} \tag{16}$$

if we also neglect exchange terms. Equation (16) can then be directly compared to

$$\begin{aligned}\frac{1}{\Delta}\frac{(1+\alpha^2)}{\gamma_0}\dot{q} &= \alpha H_{\mathrm{ext},z} \\ &\quad + M_{\mathrm{s}}\left(N_y - N_x\right)\frac{\sin 2\phi}{2}\end{aligned} \tag{17}$$

from the analytical 1D model [20]. Inspection of equations (16) and (17) learns us that $\frac{\Delta_{\mathrm{av}}}{2}$ from the semi-analytical model transforms to Δ in the 1D model. Furthermore, Φ_{av} and $M_{\mathrm{s}}(N_{\mathrm{eff},y} - N_{\mathrm{eff},x})$ transform to respectively ϕ and $M_{\mathrm{s}}\left(N_y - N_x\right)$. Consequently, we can write that

$$\frac{\langle |m_{\mathrm{ip}}|\rangle^2}{\langle m_{\mathrm{ip}}^2\rangle\zeta_{\mathrm{ms}}} = 1 \tag{18}$$

or, equivalently,

$$\zeta_{\mathrm{ms}} = \frac{\langle |m_{\mathrm{ip}}|\rangle^2}{\langle m_{\mathrm{ip}}^2\rangle}. \tag{19}$$

Since there is no straightforward way to unambiguously determine ζ_{DMI} and ζ_{exch}, we assume that they are equal to ζ_{ms}.

Consequently, we can rewrite equation (10) as

$$\begin{aligned}\frac{2}{\Delta_{\mathrm{av}}}\frac{1+\alpha^2}{\gamma_0}v(\mathbf{H}_{\mathrm{ext}}) &= \alpha H_{\mathrm{ext},z} \\ &\quad + H_{\mathrm{ext},x}\left[\frac{1}{\kappa}\sin\Phi_{\mathrm{av}}\right] - H_{\mathrm{ext},y}\left[\frac{1}{\kappa}\cos\Phi_{\mathrm{av}}\right] \\ &\quad + H_{\mathrm{d}}\left[\frac{\sin 2\Phi_{\mathrm{av}}}{2}\right]\end{aligned} \tag{20}$$

$$+ H_{\mathrm{DMI}} \left[4\kappa \left(-\sin\Phi_{\mathrm{av}} + \frac{\langle \partial_y m_z \rangle}{\langle \partial_x m_z \rangle} \cos\Phi_{\mathrm{av}} \right) \right]$$
$$+ H_{\mathrm{exch}} \left[2\Delta_{\mathrm{av}}^2 \left(\frac{\langle \partial_{xx} m_x \rangle}{\langle |m_{\mathrm{ip}}| \rangle} \sin\Phi_{\mathrm{av}} - \frac{\langle \partial_{yy} m_y \rangle}{\langle |m_{\mathrm{ip}}| \rangle} \cos\Phi_{\mathrm{av}} \right) \right],$$

thereby introducing factor

$$\kappa = \frac{\langle m_{\mathrm{ip}}^2 \rangle}{\langle |m_{\mathrm{ip}}| \rangle}, \tag{21}$$

the shape anisotropy field $H_{\mathrm{d}} = M_{\mathrm{s}}(N_{\mathrm{eff},y} - N_{\mathrm{eff},x})$, the DMI-field $H_{\mathrm{DMI}} = \frac{D_{\mathrm{DMI}}}{\mu_0 M_{\mathrm{s}} \Delta_{\mathrm{av}}}$ and the exchange field $H_{\mathrm{exch}} = \frac{A}{\mu_0 M_{\mathrm{s}} \Delta_{\mathrm{av}}^2}$. From expression (20), we now identify $\frac{\langle \partial_y m_z \rangle}{\langle \partial_x m_z \rangle}$ as

$$\tan X_{\mathrm{av}} = \frac{\langle \partial_y m_z \rangle}{\langle \partial_x m_z \rangle} \tag{22}$$

with X_{av} representing the average geometrical tilting of the DW. This variable is analogous to the collective coordinate χ introduced by Boulle *et al* [11]. Finally, we can also identify $N_{\mathrm{eff},y} - N_{\mathrm{eff},x}$, $g_x = \frac{\langle \partial_{xx} m_x \rangle}{\langle |m_{\mathrm{ip}}| \rangle}$, $g_y = \frac{\langle \partial_{yy} m_y \rangle}{\langle |m_{\mathrm{ip}}| \rangle}$ and κ as additional DW variables compared to analytical models [10, 11]. In this way, a varying $N_{\mathrm{eff},y} - N_{\mathrm{eff},x}$ takes into account the (changing) charge distribution along the DW, while g_x and g_y incorporate the effects of the exchange interaction.

We can now express (20) as

$$\begin{aligned} \frac{2}{\Delta_{\mathrm{av}}} \frac{1+\alpha^2}{\gamma_0} v(\mathbf{H}_{\mathrm{ext}}) &= \alpha H_{\mathrm{ext},z} \\ &\quad + \frac{1}{\kappa} H_{\mathrm{ext},x} \sin\Phi_{\mathrm{av}} - \frac{1}{\kappa} H_{\mathrm{ext},y} \cos\Phi_{\mathrm{av}} \\ &\quad + H_{\mathrm{d}} \frac{\sin 2\Phi_{\mathrm{av}}}{2} \\ &\quad + 4\kappa H_{\mathrm{DMI}} \left(-\sin\Phi_{\mathrm{av}} + \tan X_{\mathrm{av}} \cos\Phi_{\mathrm{av}} \right) \\ &\quad + 2\Delta_{\mathrm{av}}^2 H_{\mathrm{exch}} \left(g_x \sin\Phi_{\mathrm{av}} - g_y \cos\Phi_{\mathrm{av}} \right) \\ &= \alpha H_{\mathrm{ext},z} \\ &\quad + \left[f_{H_{\mathrm{ext},x}} + f_{H_{\mathrm{ext},y}} + f_{\mathrm{ms}} + f_{\mathrm{DMI}} + f_{\mathrm{exch}} \right]. \end{aligned} \tag{23}$$

In (23), we have introduced $f_{H_{\mathrm{ext},x}}$, $f_{H_{\mathrm{ext},y}}$, f_{ms}, f_{DMI} and f_{exch} to facilitate further discussions.

Taking into account that

$$\langle m_{\mathrm{ip}}^2 \frac{\partial \phi}{\partial t} \rangle = \langle m_x \frac{\partial m_y}{\partial t} - m_y \frac{\partial m_x}{\partial t} \rangle, \tag{24}$$

an expression that is directly derived from (7) and (12), we also derive an equation for the change in magnetization angle inside the DW

$$\begin{aligned} \frac{1+\alpha^2}{\gamma_0} \frac{\langle m_{\mathrm{ip}}^2 \frac{\partial \phi}{\partial t} \rangle}{\langle m_{\mathrm{ip}}^2 \rangle} (\mathbf{H}_{\mathrm{ext}}) &= H_{\mathrm{ext},z} \\ &\quad - \alpha \left[f_{H_{\mathrm{ext},x}} + f_{H_{\mathrm{ext},y}} + f_{\mathrm{ms}} + f_{\mathrm{DMI}} + f_{\mathrm{exch}} \right], \end{aligned} \tag{25}$$

using the functions defined in eq. (23) for compactness. Combining (23) and (25), we infer that

$$v(\mathbf{H}_{\mathrm{ext}}) + \frac{\Delta_{\mathrm{av}}}{2} \frac{1}{\alpha} \frac{\langle m_{\mathrm{ip}}^2 \frac{\partial \phi}{\partial t} \rangle}{\langle m_{\mathrm{ip}}^2 \rangle} (\mathbf{H}_{\mathrm{ext}}) = \frac{\Delta_{\mathrm{av}}}{2} \frac{\gamma_0}{\alpha} H_{\mathrm{ext},z} \tag{26}$$

which is in agreement with analytical models.

3. Field-driven domain wall motion below the Walker breakdown

3.1. Introduction

The determination of the effective fields and DW variables now eases the interpretation of the equations of motion. One can discriminate between two propagation regimes, separated by the Walker breakdown [30]. Below the WB, the DW adapts itself to the perpendicularly applied field resulting in a steady state translational motion along the nanostrip. In the equations of motion, this corresponds to

$$\langle m_{\mathrm{ip}}^2 \frac{\partial \phi}{\partial t} \rangle = 0, \tag{27}$$

i.e. a fixed magnetization.

Under these conditions, the left hand side of equation (25) is zero and thus

$$\alpha \left[f_{\mathrm{ms}} + f_{\mathrm{DMI}} + f_{H_{\mathrm{ext},x}} + f_{H_{\mathrm{ext},y}} + f_{\mathrm{exch}} \right] = H_{\mathrm{ext},z}. \tag{28}$$

This expression shows how the different interactions (left hand side) add up to balance the externally applied driving field (right hand side). As long as these interactions can balance $H_{\mathrm{ext},z}$, we are below the WB. If the signs of an interaction contribution and the externally applied driving field are different, this contribution has an opposing influence: other contributions have to be larger to balance the driving field. On the other hand, if the signs of an interaction contribution and the externally applied driving field are the same, this contribution has a reinforcing influence.

To avoid confusion in the further discussion, we want to emphasize the difference between the magnetization angle and the magnetization tilting: while the magnetization angle simply corresponds to Φ_{av}, the magnetization tilting corresponds to $|\Phi_{\mathrm{av}} - \Phi_{\mathrm{av},0}|$ with $\Phi_{\mathrm{av},0} = \Phi_{\mathrm{av}}(H_{\mathrm{ext},z} = 0)$.

3.2. Detailed analysis

3.2.1. Micromagnetic simulations To evaluate the equations of motion and the collective coordinates, we performed micromagnetic simulations using the micromagnetic software package MuMax^3 [31]. The chosen material parameters were $M_{\mathrm{s}} = 1090 \times 10^3\,\mathrm{A/m}$, exchange stiffness $A = 1 \times 10^{-11}\,\mathrm{J/m}$, anisotropy constant $K_{\mathrm{u}} = 1.25 \times 10^6\,\mathrm{J/m^3}$ and Gilbert damping parameter $\alpha = 0.2$. The cross sectional dimensions of the simulated nanostrip were $100 \times 0.6\ \mathrm{nm}^2$ while the simulation window was restricted to an area of length 400 nm following the DW in its propagation through an infinite nanostrip. Furthermore, D_{DMI} were varied between -1 and 1 $\mathrm{mJ/m^2}$, while $\mu_0 H_{\mathrm{ext},x}$ was changed between -20 and 20 mT. The discretization cells had the dimensions $1.5625 \times 1.5625 \times 0.6\ \mathrm{nm}^3$. A fourfold decrease of the cell sizes generated very similar simulation results (differences smaller than 2 %) as expected since $\sqrt{A/K} \approx 2.83$ nm. However, when calculating the averages, interpolation was used to compensate for discretization effects as discussed in Appendix A.

3.2.2. Influence of in-plane and out-of-plane fields In this subsubsection, we focus on DW dynamics for varying out-of-plane fields $|H_{\mathrm{ext},z}| \leq |H_{\mathrm{WB}}|$ with a fixed DMI strength $D_{\mathrm{DMI}} = 0.4\ \mathrm{mJ/m^2}$ and in-plane fields varying between -20 mT and 20 mT.

First, we determine the contributions of the magnetostatic, exchange and DM interactions and in-plane fields to balancing a driving field $H_{\mathrm{ext},z}$. Since the

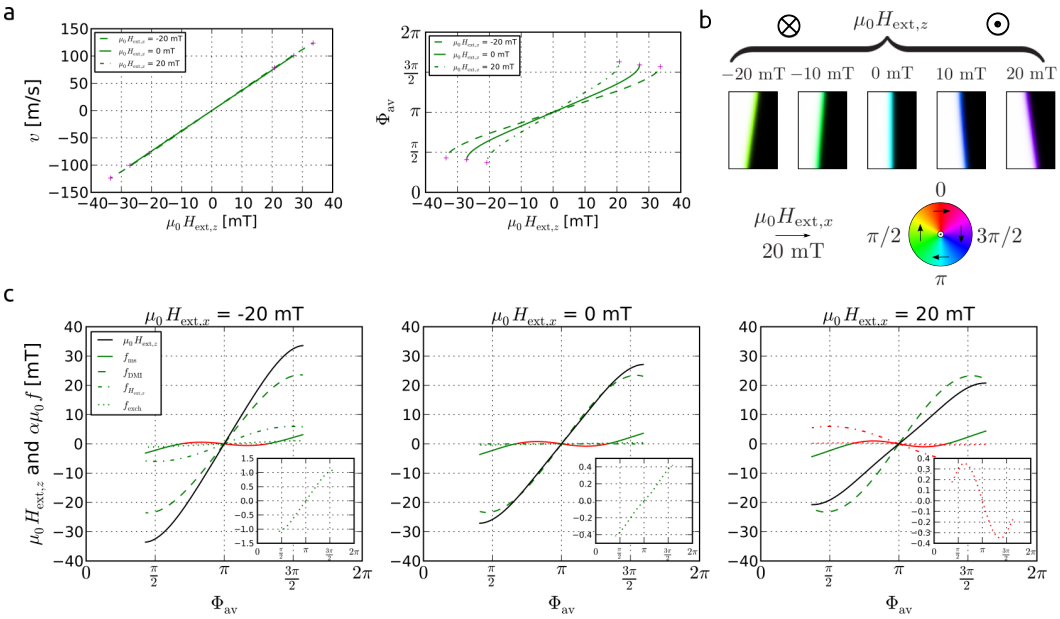

Figure 2. Magnetostatic, exchange, DM interactions and in-plane fields in the case of DW dynamics for fields $|\mu_0 H_{\text{ext},z}| \leq |\mu_0 H_{\text{WB}}|$ in a nanostrip with $D_{\text{DMI}} = 0.4$ mJ/m^2 and varying in-plane fields. (a) The DW velocity v and magnetization tilting Φ_{av} as a function of the driving field $\mu_0 H_{\text{ext},z}$. Also the points corresponding to $|\mu_0 H_{\text{WB}}|$ are identified; (b) Snapshots showing the magnetization of the DW at $\mu_0 H_{\text{ext},z}$ ranging from -20 mT to 20 mT when the in-plane field $\mu_0 H_{\text{ext},x} = 20$ mT and corresponding color code linking color to magnetization angle; (c) $\mu_0 H_{\text{ext},z}$, $\alpha\mu_0 f_{\text{ms}}$, $\alpha\mu_0 f_{\text{DMI}}$, $\alpha\mu_0 f_{H_{\text{ext},x}}$, $\alpha\mu_0 f_{\text{exch}}$ from equation (28) versus Φ_{av} for three different in-plane fields: $\mu_0 H_{\text{ext},x} = -20$ mT (left), $\mu_0 H_{\text{ext},x} = 0$ mT (middle) and $\mu_0 H_{\text{ext},x} = 20$ mT (right). Subplots are included depicting $\alpha\mu_0 f_{\text{exch}}$ as a function of Φ_{av}. The red lines indicate an interaction opposing the driving field, while the green lines highlight interactions reinforcing the driving field.

magnetization angle Φ_{av} is a variable occurring in every term of (28), we chose to plot all internal fields as a function of Φ_{av}. Fig. 2 (a) shows how the DW velocity v and Φ_{av} relate to $\mu_0 H_{\text{ext},z}$ while Fig. 2 (c) shows the different terms from (28) as a function of Φ_{av} for the different in-plane fields. The red lines indicate an interaction opposing the driving field, while the green lines highlight interactions reinforcing the driving field.

From Fig. 2 (c), it is clear that f_{DMI} is the largest interaction contribution. Consequently, f_{DMI} strongly influences the DW magnetization and its shape. In this respect, we notice that in the observed cases $\Phi_{\text{av},0} = \pi$, i.e. the DW magnetization is initially in the negative x-direction (Néel wall), while we also notice that the magnetization tilting at the WB is beyond $\pi/2$. This contrasts typical PMA nanostrips without DMI. There, the magnetization of the DW is initially in the positive/negative y-direction (Bloch wall) [32] and the magnetization tilting at breakdown is only at around $\pi/4$ [23]. Furthermore, f_{DMI} strongly reinforces the driving field, significantly enhancing the DW speed at the WB [10].

Fig. 2 also shows that $f_{H_{\mathrm{ext},x}}$ has a reinforcing role when $\mu_0 H_{\mathrm{ext},x} = -20$ mT. Indeed, when the in-plane field is in the same direction (negative x-direction) as the initial DW magnetization (negative x-direction), more energy is needed to tilt the DW, thereby reinforcing the DW magnetization. This is in accordance with the magnetization tilting $|\Phi_{\mathrm{av}} - \Phi_{\mathrm{av},0}|$ found at lower values for a fixed $|\mu_0 H_{\mathrm{ext},z}| \neq 0$ and the significant increase of the WB field. On the other hand, the magnetization tilting at WB is generally smaller due to the in-plane field and the DW magnetization opposing each other. When $\mu_0 H_{\mathrm{ext},x} = 20$ mT, the situation is vice versa. Note that, while the WB and the DW magnetization are significantly affected, the DW velocity is only barely affected by an additional in-plane field for a fixed $|\mu_0 H_{\mathrm{ext},z}| \neq 0$ below the Walker breakdown.

Furthermore, we perceive that f_{exch} reinforces or opposes the driving field, depending on the in-plane field, but is much smaller than the other contributions. On the other hand, f_{ms} reinforces [opposes] the driving field when the magnetization tilting is high [low]. Finally, we also perceive that while the in-plane field $\mu_0 H_{\mathrm{ext},x}$ has a strong effect on $f_{H_{\mathrm{ext},x}}$ and f_{exch}, the effect is less pronounced for f_{ms} and barely visible for f_{DMI}, except with respect to the range of Φ_{av}.

In Fig. 3, the DW deformations are quantified in terms of the DW variables in an attempt to clarify the influence of the external fields.

While $|X_{\mathrm{av}}|$ strongly increases with increasing magnetization tilting $|\Phi_{\mathrm{av}} - \Phi_{\mathrm{av},0}|$ in accordance with Fig. 2 (b), it is almost unaffected by in-plane fields. This is in agreement with what we expect from the effect of in-plane fields on $f_{\mathrm{DMI}}(\Phi_{\mathrm{av}})$. Moreover, we verified that X_{av} indeed corresponds to a geometrical tilting by comparing it with the angle of the line $m_z = 0$ as illustrated in Fig. 1 (b). The first term of f_{DMI} ($\sim \sin\Phi_{\mathrm{av}}$) is the main term in reinforcing the driving field and decreases for a DW magnetization tilting beyond $\pi/2$. However, since $|\tan X_{\mathrm{av}}|$ (second term $\sim \tan X_{\mathrm{av}} \cos\Phi_{\mathrm{av}}$) increases with increasing out-of-plane field $|\mu_0 H_{\mathrm{ext},z}|$ and since f_{ms} is largest when $\Phi_{\mathrm{av}} \approx \pm\pi/4$ i.e. in the middle of a Bloch-Néel transition, the significant magnetization tilting beyond $\pi/2$ at the WB is as expected.

The evolution of Δ_{av} is partially due to the increase of $\langle m_{\mathrm{ip}}^2 \rangle$ with increasing X_{av}. To increase insight in DW dynamics, we define a net DW width

$$\Delta_{\mathrm{av,net}} = \Delta_{\mathrm{av}} \cos X_{\mathrm{av}}, \tag{29}$$

that compensates for the effect of X_{av}, based on simple geometric rules. The variation of $\Delta_{\mathrm{av,net}}$ can then be understood from the interplay between the in-plane field direction and the DW magnetization: the smaller the angle between the DW magnetization and the in-plane field direction, the wider the DW. However, when there is no in-plane field, the largest [smallest] net DW width is associated with a Néel [Bloch] DW [23]. At $|\Phi_{\mathrm{av}} - \Phi_{\mathrm{av},0}| = \pi/2$, all curves cross as expected. Note that, while there is a clear variation in the evolution of $\Delta_{\mathrm{av,net}}$ as a function of Φ_{av}, this variation is small in absolute terms. This is in accordance with the combination of equation (26) with the observation that the DW velocity v barely changes as a function of $\mu_0 H_{\mathrm{ext},z}$.

The alternate reinforcing/opposing role of f_{ms} is understood from the evolution of $\frac{\sin 2\Phi_{\mathrm{av}}}{2}$ and $N_{\mathrm{eff},y} - N_{\mathrm{eff},x}$ through H_{d}, see (23). $N_{\mathrm{eff},y} - N_{\mathrm{eff},x}$ is related to both the magnetization tilting, the geometric tilting angle X_{av} and the net domain wall width $\Delta_{\mathrm{av,net}}$, explaining why there is barely difference for the different in-plane fields as a function of the magnetization angle. The factor $\kappa \approx 2/3$ is approximately constant,

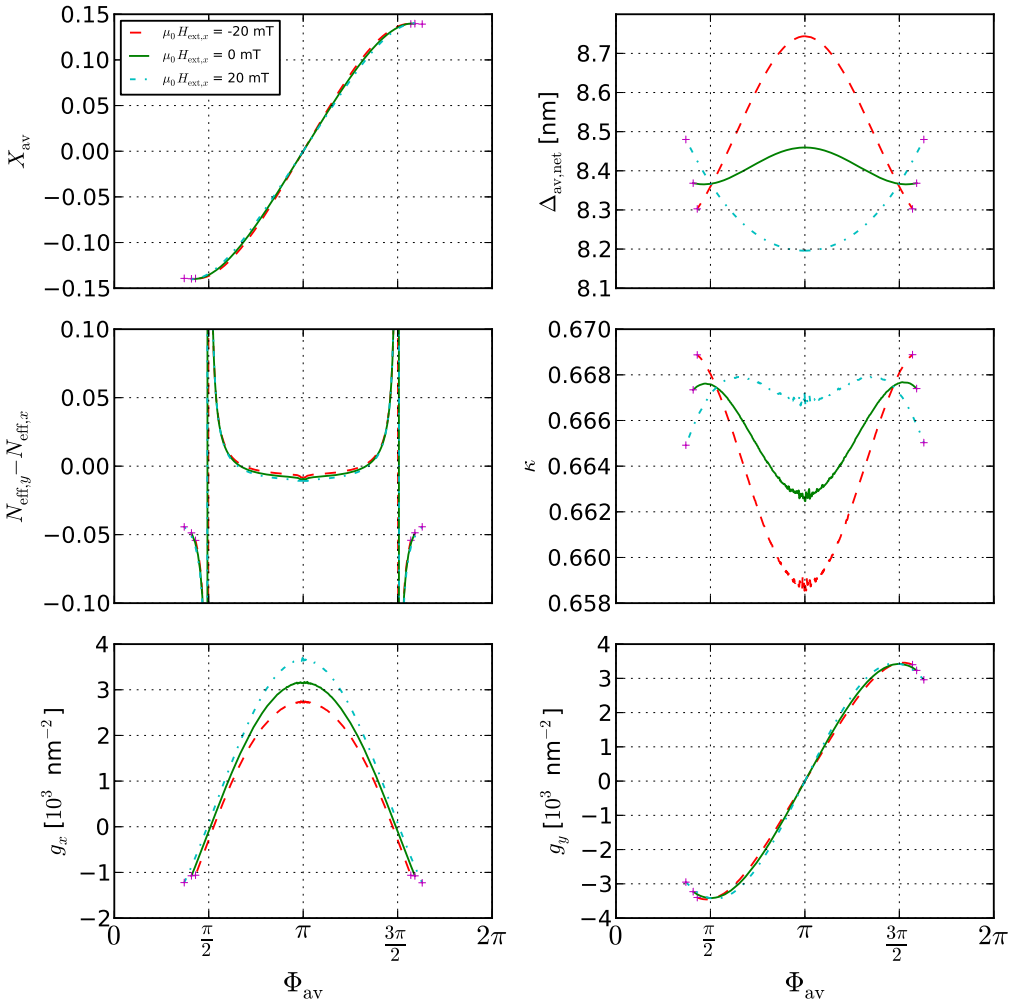

Figure 3. DW variables in the equations of motion for fields $|\mu_0 H_{\mathrm{ext},z}| \leq |\mu_0 H_{\mathrm{WB}}|$ in a nanostrip with $D_{\mathrm{DMI}} = 0.4$ mJ/m^2 and varying in-plane fields. From top-left to bottom-right: the geometrical tilting X_{av}, the net DW width $\Delta_{\mathrm{av,net}}$ – defined in (29) and compensating for the influence of X_{av}, $N_{\mathrm{eff},y} - N_{\mathrm{eff},x} = \frac{H_{\mathrm{d}}}{M_{\mathrm{s}}}$, κ, g_x and g_y from equation (23) versus Φ_{av}. Also the points corresponding to $|\mu_0 H_{\mathrm{WB}}|$ are identified.

while g_x and g_y evolve approximately with $-\cos\Phi_{\mathrm{av}}$ and $-\sin\Phi_{\mathrm{av}}$, respectively. Combined with (23), this clarifies why both exchange terms almost cancel each other, resulting in a relatively small f_{exch}. f_{exch} is different for different in-plane fields, given a fixed angle $\Phi_{\mathrm{av}} \neq \pi$, since $|g_x|$ is larger [smaller] when the in-plane field is in the opposite [same] direction as the initial magnetization direction, while $|g_y|$ is barely affected by the in-plane fields considered here.

3.2.3. Influence of DMI strength We now discuss the influence of the DMI strength on DW dynamics for a constant longitudinal field. We mainly focus on the dynamics at WB as it is of particular interest for the development of technologies based on fast DW propagation. In the following, we restrict ourselves to the situation with $\mu_0 H_{\mathrm{ext},x} = 20$ mT, but discussions considering other in-plane fields of the same order of magnitude are analogous.

In Fig. 4(a), the driving force field $|\mu_0 H_{\mathrm{ext},z}|$ is plotted for varying DMI strengths as a function of Φ_{av}. The plots demonstrate that at fixed tilting angle $\Phi_{\mathrm{av}} \neq \Phi_{\mathrm{av},0}$ $|\mu_0 H_{\mathrm{ext},z}|$ is larger when $|D_{\mathrm{DMI}}|$ is larger. We also observe that a sufficiently large in-plane field $\mu_0 H_{\mathrm{ext},x} = 20$ mT breaks the symmetry between positive and negative DMI strengths, resulting in a positive [negative] shift in WB field and corresponding velocity when the DMI strength is negative [positive]. This is naturally expected from the interplay between the in-plane field direction and the DW magnetization direction. Moreover, this is in accordance with Fig. 4(c) plotting the different relative contributions of (25) as a function of D_{DMI} at the WB field $\mu_0 H_{z,\mathrm{WB}}$. For negative DMI strengths, all contributions reinforce the driving field. On the other hand, for positive DMI strengths, $f_{\mathrm{H_{ext,x}}}$ consistently opposes the driving field.

Fig. 4(c) clearly shows that, for increasing absolute DMI strengths, the relative importance of $f_{\mathrm{H_{ext,x}}}$ and f_{exch} at the WB strongly decreases, while the relative effect of f_{ms} slightly decreases. The significant decrease of the relative influence of $f_{\mathrm{H_{ext,x}}}$ at WB can be understood from $f_{\mathrm{H_{ext,x}}} \propto H_{\mathrm{ext},x}\sin\Phi_{\mathrm{av}}$ in combination with the only slightly varying magnetization tilting, taking into account the strong increase in $\mu_0 H_{z,\mathrm{WB}}$. The magnetization tilting $|\Phi_{\mathrm{av,WB}} - \Phi_{\mathrm{av},0}|$ is generally larger for positive DMI strengths due to the in-plane field reinforcing the DW magnetization at WB and vice versa for negative DMI strengths as can be observed from the polar plots. The variation of $|\Phi_{\mathrm{av,WB}} - \Phi_{\mathrm{av},0}|$ for a fixed sign of DMI can then be understood from the interplay between 2 effects, in accordance with the discussion in Subsubsection 3.2.2:

- For increasing DMI strengths, the second term of f_{DMI} ($\sim \tan X_{\mathrm{av}}\cos\Phi_{\mathrm{av}}$) has a larger contribution in reinforcing the driving field since X_{av} is then larger (not shown here), thereby compensating more for the decrease of the first term of f_{DMI} beyond $\pi/2$ ($\sim \sin\Phi_{\mathrm{av}}$).
- For lower DMI strengths, the magnetostatic field has a larger influence on the magnetization tilting, which is especially clear for positive DMI strengths. This field reaches a maximum when the magnetization tilting is around $3\pi/4$.

The increase of $X_{\mathrm{av,WB}}$ as a function of increasing $|D_{\mathrm{DMI}}|$ is a consequence of the increasing impact of f_{DMI} and accordingly the increasing out-of-plane fields at the WB, enabling a larger deformation of the DW. Moreover, this increasing $X_{\mathrm{av,WB}}$ is strongly related to the shape of the DW and hence, the magnetic charges throughout the DW. This affects then $N_{\mathrm{eff},y,WB} - N_{\mathrm{eff},x,WB}$ (not shown here) and accordingly $f_{\mathrm{ms,WB}}$, explaining why the relative effect of $f_{\mathrm{ms,WB}}$ is still significant for larger DMI

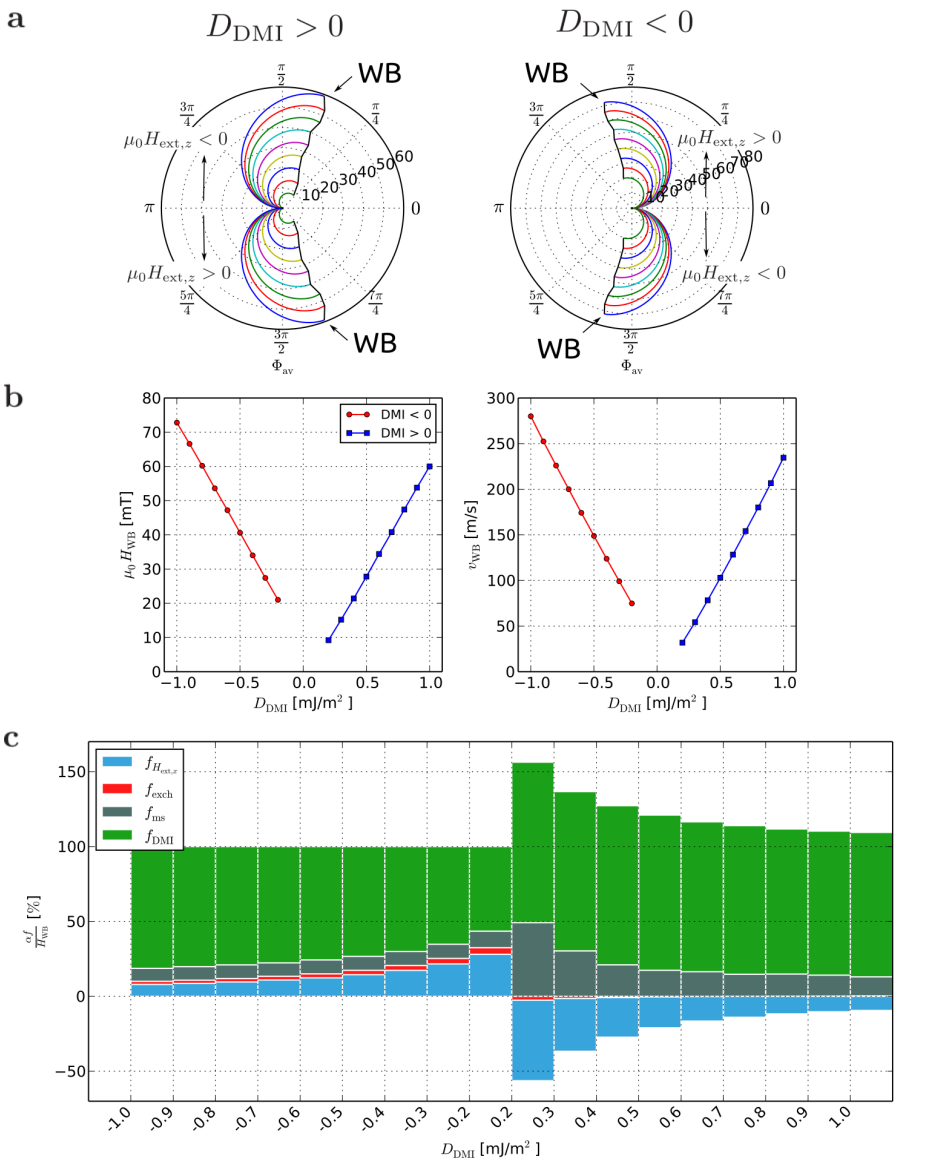

Figure 4. Figure comparing DW dynamics for varying DMI strengths when a DW is driven by out-of-plane fields in a nanostrip with $\mu_0 H_{\mathrm{ext},x} = 20$ mT. (a) Polar plots (upper part) displaying $|\mu_0 H_{\mathrm{ext},z}|$ as a function of Φ_{av} where the different colors correspond to varying DMI strengths starting from green ($|D_{\mathrm{DMI}}| = 0.2$ mJ/m^2) in steps of 0.1 mJ/m^2 to blue ($|D_{\mathrm{DMI}}| = 1$ mJ/m^2), thereby discriminating between $D_{\mathrm{DMI}} > 0$, $D_{\mathrm{DMI}} < 0$. Moreover, it is illustrated how to read these plots when $\mu_0 H_{\mathrm{ext},z} > 0$ and $\mu_0 H_{\mathrm{ext},z} < 0$, respectively and the lines corresponding to the WB field $|\mu_0 H_{\mathrm{WB}}|$ are identified. (b) The WB field and its corresponding velocity as a function of DMI strength. (c) How the different interaction contributions $\alpha\mu_0 f_{\mathrm{ms}}$, $\alpha\mu_0 f_{\mathrm{DMI}}$, $\alpha\mu_0 f_{H_{\mathrm{ext},x}}$, $\alpha\mu_0 f_{\mathrm{exch}}$ from equation (28) relatively compensate for the WB field $\mu_0 H_{\mathrm{WB}}$ as a function of DMI strength.

strengths. Furthermore, we found that $|g_y|$ and $\Delta_{\mathrm{av,net}}$ slightly increase as a function of Φ_{av} with increasing $|D_{\mathrm{DMI}}|$, while $|g_x|$ barely changes. This explains why $f_{\mathrm{exch,WB}}$ increasingly reinforces/decreasingly opposes the driving field with increasing $|D_{\mathrm{DMI}}|$. Note that this is not in contradiction with Fig. 4(c) that only shows the relative importance of the different interactions.

4. Conclusions

In this paper, we introduced a semi-analytical approach to investigate the effect of DMI on field-driven DW motion. We spatially averaged the Landau-Lifshitz-Gilbert equation, resulting in equations of motion with variables for the DW properties. Next to the DW position, seven DW variables were identified from the equations of motion. This contrasts analytical models where DW variables are introduced in an ansatz describing the DW shape [11, 20]. However, these variables could be compared, but that is out of the scope of this work.

The equations of motion clearly showed how the interaction contributions add up to balance the out-of-plane driving field. To quantify these contributions, we used micromagnetic simulations. Their reinforcing/opposing effect was then investigated for varying out-of-plane fields and several in-plane fields to gain more insight in the effect of DMI. An accompanying interpretation was given based on the variables. Furthermore, we investigated the relative importance of these interactions at the WB as a function of varying DMI strength. This helps to understand how the WB may be delayed leading to the realization of higher DW velocities.

Acknowledgments

Research funded by a Ph.D. grant of the Agency for Innovation by Science and Technology (IWT). B. Van de Wiele acknowledges financial support from the Flanders Research Foundation (FWO). Financial support was also provided by Ghent University (BOF-project 01J16113). This study was conducted as part of the Marie Curie ITN WALL project, which has received funding from the European Unions Seventh Framework Programme for research, technological development and demonstration under grant agreement no. 608031.

Appendix A. Defining the averaging window

In order to accurately describe the DW behaviour using the methodology presented in this work, the averages $\langle f \rangle$ have to be calculated in a proper way. In perpendicularly magnetized nanostrips without DMI and in-plane fields, the domain magnetization has no in-plane magnetized contributions as depicted in Figure 1(a). The DW position Q is then expressed as [27]

$$Q(t) = \frac{L_x}{2} \langle m_z(\mathbf{r}, t) \rangle \tag{A.1}$$

with the average $\langle f \rangle$ taken over any volume of the nanostrip including the DW [23–25]. Taking into account that DMI leads to edge effects and in-plane fields lead to magnetization canting of the domains as depicted in Figure 1(b-d), eq. (A.1) is replaced by

$$Q(t) = \frac{1}{-\langle \partial_x m_z(\mathbf{r}, t) \rangle} \langle m_z(\mathbf{r}, t) \rangle. \tag{A.2}$$

While the DW position Q is well defined by (A.2) for every averaging window that includes the DW, both effects undesirably affect the evaluation of the equations of motion when a significant part of the domains is taken into account. For example, Δ_{av} defined as

$$\Delta_{\mathrm{av}} \equiv 2\frac{\langle m_{\mathrm{ip}}^2\rangle}{-\langle\partial_x m_z\rangle} \tag{A.3}$$

and Φ_{av} determined by

$$\tan\Phi_{\mathrm{av}} = \frac{\langle m_y\rangle}{\langle m_x\rangle}, \tag{A.4}$$

then lose their meaning as respectively the DW width (the DW width is then overestimated) and magnetization angle inside the DW (this angle is then underestimated or overestimated). Therefore, $\langle f\rangle$ is by definition restricted to the DW

$$\langle f\rangle(t) = \frac{1}{V_{\mathrm{DW}}}\int\int\int_{V_{\mathrm{DW}}} f(\mathbf{r},t)\,\mathrm{d}V \tag{A.5}$$

with V_{DW} the DW volume as schematically represented in Fig. 1 (b) and rigorously defined further in this appendix. Since we neglect DW asymmetry, this implies that $\langle m_z\rangle(t) = 0$ and thus $Q(t) = 0$ at every timestep t in accordance with equation (A.2). However, we can still have a nonzero DW velocity derived as

$$v(t) \equiv \frac{\mathrm{d}Q(t)}{\mathrm{d}t}. \tag{A.6}$$

To prove this, we elaborate equation (A.6)

$$\begin{aligned} v(t) &= \frac{1}{-\langle\partial_x m_z\rangle(t)}\frac{\mathrm{d}\langle m_z\rangle(t)}{\mathrm{dt}} \\ &\quad + \frac{\langle m_z\rangle(t)}{\langle\partial_x m_z\rangle^2(t)}\frac{\mathrm{d}\langle\partial_x m_z\rangle(t)}{\mathrm{dt}} \\ &= \frac{1}{-\langle\partial_x m_z\rangle(t)}\frac{\mathrm{d}\langle m_z\rangle(t)}{\mathrm{dt}}, \end{aligned} \tag{A.7}$$

thereby taking into account equation (A.2) and $\langle m_z\rangle(t) = 0$. Furthermore, we rewrite equation (A.7) as

$$v(t) = \lim_{\Delta t\to 0}\frac{1}{-\langle\partial_x m_z(t)\rangle}\frac{\langle m_z\rangle(t+\Delta t) - \langle m_z\rangle(t)}{\Delta t} \tag{A.8}$$

with

$$\langle m_z\rangle(t+\Delta t) = \frac{1}{V_{\mathrm{DW}}(t)}\int\int\int_{V_{\mathrm{DW}}} m_z(\mathbf{r},t+\Delta t)\,\mathrm{d}V. \tag{A.9}$$

Since the DW volume $V_{\mathrm{DW}}(t)$ is only evaluated at timestep t, equation (A.9) implies that $\langle m_z\rangle(t+\Delta t)$ can be different from zero with respect to this DW volume resulting in a nonzero DW velocity.

In order to define the DW volume V_{DW} in (A.5), we fix the left boundary based on m_z changing only significantly inside the DW as a function of x

$$|\partial_x m_z| \geq \epsilon\,[\mathrm{nm}^{-1}] \tag{A.10}$$

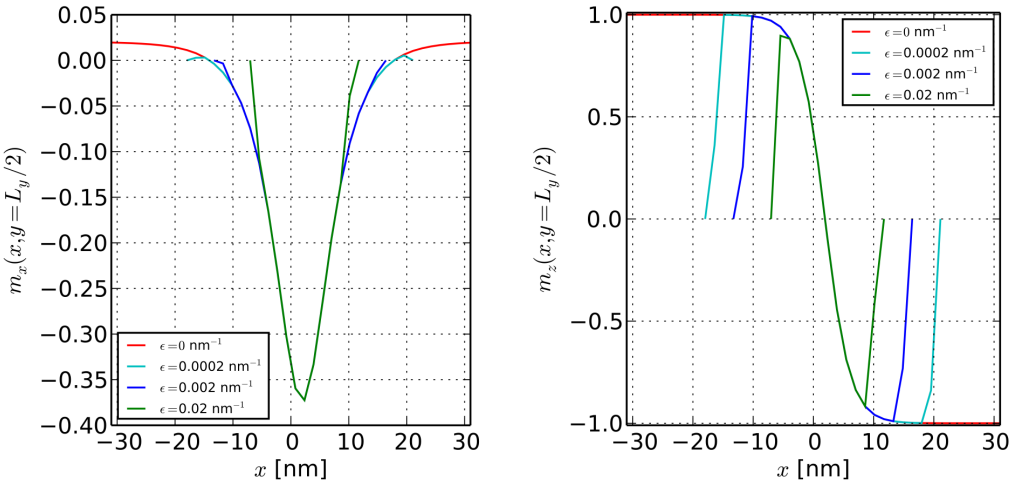

Figure A1. Left [right] part compares the curves plotting m_x [m_z] along the middle of the nanostrip ($y = \frac{L_y}{2}$) as a function of x for several ϵ-values fulfilling condition (A.10), defining the left-boundary of the averaging window, together with condition (A.11), defining the right boundary of the averaging window, when a DW is moved through a nanostrip with $D_{\mathrm{DMI}} = 0.4$ mJ/m^2, $\mu_0 H_{\mathrm{ext},x} = 20$ mT, $\mu_0 H_{\mathrm{ext},z} = 15$ mT, $L_y = 100$ nm and $L_z = 0.6$ nm, see also Fig. 1. Note that the case $\epsilon = 0$ nm^{-1} corresponds to the averaging window being the same as the computational window.

with ϵ a well-chosen constant, while the right boundary of the averaging window is fixed by stating that

$$\int_{\mathrm{DW}} m_z(\mathbf{r}, t)\, \mathrm{d}x = 0 \tag{A.11}$$

should be fulfilled in every y-row. If ϵ is too large, only a small part of the DW is taken into account, thereby neglecting the full complexity of the DW. On the other hand, if ϵ is too small, a significant part of the domains is taken into account causing unwanted contributions to the averages. In Fig. A1, we compare the curves plotting m_x and m_z as a function of x at $y = \frac{L_y}{2}$ for several ϵ-values ($\epsilon = 0$, 0.0002, 0.002 and 0.02 nm^{-1}). Based on Fig. A1 and other results (e.g. we want to assure that $\max\left(\left|\frac{\langle m_x\rangle}{\langle|m_{\mathrm{ip}}|\rangle}\right|\right) = 1$ and $\max\left(\left|\frac{\langle m_y\rangle}{\langle|m_{\mathrm{ip}}|\rangle}\right|\right) = 1$), we choose $\epsilon = 0.002$. This value is used consistently in this paper. Note that ϵ is not a sensitive parameter, so other values of ϵ (of the same order of magnitude) can be chosen. Therefore, it is important that the definitions for the DW velocity and DW width given by respectively (A.7) and (A.3) give rise to similar results for slightly varying ϵ-values. While a higher ϵ implies a smaller averaging window, it also results in a smaller increase/decrease of $V_{\mathrm{DW}}\langle m_z\rangle$ at a fixed time interval and a smaller $V_{\mathrm{DW}}\langle m_{\mathrm{ip}}^2\rangle$. This is then compensated by a smaller $V_{\mathrm{DW}}|\langle\partial_x m_z\rangle|$ in the denominator. Note that for every average $\langle.\rangle$ in the numerator, there is an average $\langle.\rangle$ in the denominator, so the multiplication of $\langle.\rangle$ with V_{DW} in our argumentation is allowed.

Every timestep, the averaging window is redefined and the averages are computed with high precision using interpolation to minimize discretization effects. On every

timestep, we first construct matrices with as many cells as the computational window (dimensions $L_x \times L_y \times L_z$) for each relevant average and save the quantities in every cell without making any assumptions. To correctly calculate these quantities, boundary conditions are also taken into account [31]. This way, also a m_z-matrix is constructed. Based on this matrix we define the averaging window by evaluating (A.10) and (A.11) at every y-row. Next, every cell from the original matrix which is not part of the averaging window is set zero while the other cells retain their value. Interpolation using weight factors is used to define the value of the cells at the edges of the averaging window. Finally, the averages are calculated by summing the nonzero cells of the modified matrices and dividing this sum by the weighted number of nonzero cells.

Appendix B. Domain wall asymmetry

If we rewrite (6) and the temporal derivative of (7) by explicitly evaluating and averaging equation (1) after inserting (8), we get expressions for the DW velocity and the change of magnetization in terms of DW variables. More specifically, using the expression $m_x^2 + m_y^2 + m_z^2 = 1$, we derive the following description for the DW velocity

$$
\begin{aligned}
&-\frac{\langle \partial_x m_z \rangle}{\langle m_{\mathrm{ip}}^2 \rangle} \frac{1+\alpha^2}{\gamma_0} v(\mathbf{H}_{\mathrm{ext}}) = \\
&\left[H_{\mathrm{ext},x} \frac{\langle m_y \rangle}{\langle m_{\mathrm{ip}}^2 \rangle} - H_{\mathrm{ext},y} \frac{\langle m_x \rangle}{\langle m_{\mathrm{ip}}^2 \rangle} + \alpha \left(H_{\mathrm{ext},z} - H_{\mathrm{ext},x} \frac{\langle m_x m_z \rangle}{\langle m_{\mathrm{ip}}^2 \rangle} - H_{\mathrm{ext},y} \frac{\langle m_y m_z \rangle}{\langle m_{\mathrm{ip}}^2 \rangle} \right) \right] \\
&+\alpha \frac{2K_{\mathrm{u}}}{\mu_0 M_{\mathrm{s}}} \frac{\langle m_z \rangle}{\zeta_{\mathrm{ani}}} \\
&+M_{\mathrm{s}} \left[(N_{\mathrm{eff},y} - N_{\mathrm{eff},x}) \frac{\langle m_x \rangle \langle m_y \rangle}{\langle m_{\mathrm{ip}}^2 \rangle \zeta_{\mathrm{ms}}} + \alpha \left(N_{\mathrm{eff},x} \frac{\langle m_x \rangle \langle m_x m_z \rangle}{\langle m_{\mathrm{ip}}^2 \rangle \zeta_{\mathrm{ms}}} + N_{\mathrm{eff},y} \frac{\langle m_y \rangle \langle m_y m_z \rangle}{\langle m_{\mathrm{ip}}^2 \rangle \zeta_{\mathrm{ms}}} - N_{\mathrm{eff},z} \frac{\langle m_z \rangle}{\zeta_{\mathrm{ms}}} \right) \right] \\
&+\frac{2D_{\mathrm{DMI}}}{\mu_0 M_{\mathrm{s}}} \left[\frac{\langle \partial_x m_z \rangle \langle m_y \rangle}{\langle m_{\mathrm{ip}}^2 \rangle \zeta_{\mathrm{DMI}}} - \frac{\langle \partial_y m_z \rangle \langle m_x \rangle}{\langle m_{\mathrm{ip}}^2 \rangle \zeta_{\mathrm{DMI}}} - \alpha \left(\frac{\langle \partial_x m_z \rangle \langle m_x m_z \rangle}{\langle m_{\mathrm{ip}}^2 \rangle \zeta_{\mathrm{DMI}}} + \frac{\langle \partial_y m_z \rangle \langle m_y m_z \rangle}{\langle m_{\mathrm{ip}}^2 \rangle \zeta_{\mathrm{DMI}}} + \frac{\langle \partial_x m_x + \partial_y m_y \rangle}{\zeta_{\mathrm{DMI}}} \right) \right] \\
&+\frac{2A}{\mu_0 M_{\mathrm{s}}} \left[\frac{\langle \partial_{xx} m_x \rangle \langle m_y \rangle}{\langle m_{\mathrm{ip}}^2 \rangle \zeta_{\mathrm{exch}}} - \frac{\langle \partial_{yy} m_y \rangle \langle m_x \rangle}{\langle m_{\mathrm{ip}}^2 \rangle \zeta_{\mathrm{exch}}} - \alpha \left(\frac{\langle \partial_{xx} m_x \rangle \langle m_x m_z \rangle}{\langle m_{\mathrm{ip}}^2 \rangle \zeta_{\mathrm{exch}}} + \frac{\langle \partial_{yy} m_y \rangle \langle m_y m_z \rangle}{\langle m_{\mathrm{ip}}^2 \rangle \zeta_{\mathrm{exch}}} - \frac{\langle \partial_{zz} m_z \rangle}{\zeta_{\mathrm{exch}}} \right) \right]
\end{aligned}
\tag{B.1}
$$

with $\mathbf{m}_{\mathrm{ip}}$ a magnetization vector that only takes into account the in-plane magnetization

$$\mathbf{m}_{\mathrm{ip}} \equiv m_x \mathbf{e}_x + m_y \mathbf{e}_y. \tag{B.2}$$

From this equation, we immediately get that

$$\langle m_{\mathrm{ip}}^2 \rangle = \langle m_x^2 + m_y^2 \rangle \tag{B.3}$$

and

$$\langle |m_{\mathrm{ip}}| \rangle \equiv \langle \sqrt{m_x^2 + m_y^2} \rangle. \tag{B.4}$$

The equations can be simplified taking into account that integration over odd functions results in zero. When the DW is symmetric – see Fig. B1 for the definition of symmetry– $m_z(x,y)$, $\partial_x m_x(x,y)$ and $\partial_{zz} m_z(x,y)$ are odd functions while $m_x(x,y)$,

$m_y(x,y)$, $\partial_x m_z(x,y)$, $\partial_{xx} m_x(x,y)$ and $\partial_{yy} m_y(x,y)$ are even functions in the x-direction. When the DW is geometrically tilted, see Fig. 1, $\partial_y m_y(x,y)$ is an odd function while $\partial_y m_z(x,y)$ is an even function in the x-direction. On the other hand, when the DW is asymmetric, integration over these functions results in non-zero contributions.

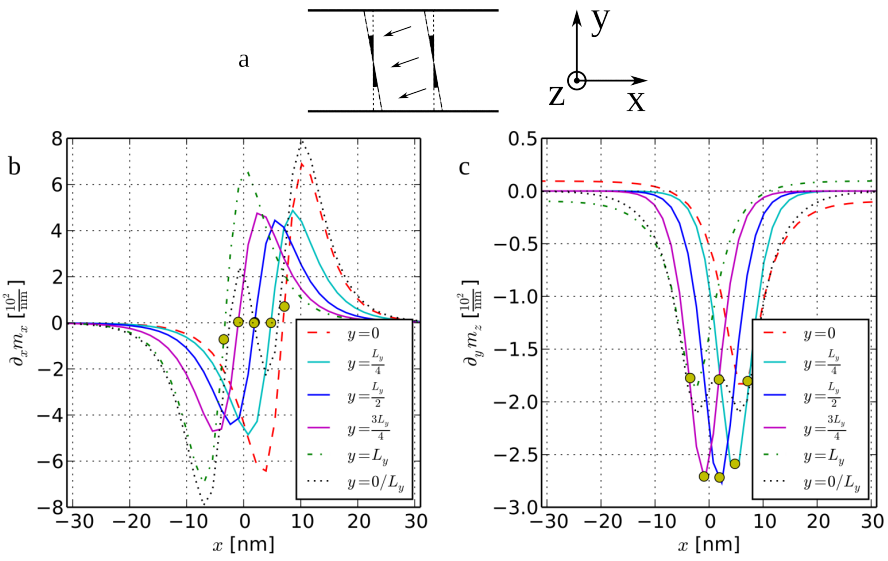

Figure B1. A symmetric DW in an out-of-plane magnetized nanostrip is defined as a DW in which the magnetization, for every y-value (except at the edges) as a function of x with $m_z = 0$ corresponding to $x = 0$, is (i) an odd function when considering the magnetization in the z-direction and (ii) an even function when considering the magnetization in the x-and y-direction. Moreover, the sum of the values at both edges as a function of x should also result in (i) odd or (ii) even functions, respectively. A sketch of a typical symmetric DW is depicted in (a). In (b) and (c), $\partial_x m_x(x,y)$ and $\partial_y m_z(x,y)$ are plotted for $y = 0$ (bottom nanostrip), $y = \frac{L_y}{4}$, $y = \frac{L_y}{2}$ (middle nanostrip), $y = \frac{3L_y}{4}$ and $y = L_y$ (top nanostrip) as a function of x in the case that a DW is moved through a nanostrip with $D_{\text{DMI}} = 0.4$ mJ/m^2, $\mu_0 H_{\text{ext},x} = 20$ mT, $\mu_0 H_{\text{ext},z} = 15$ mT, $L_y = 100$ nm and $L_z = 0.6$ nm. The points that correspond to $m_z = 0$ are indicated as yellow dots. With respect to these points, curves are (b) odd and (c) even, except at the edges. However, if we sum the values at the edges ($y = 0/L_y$), the resulting curves are also (b) odd and (c) even, indicating that such a DW is symmetric in accordance with what we expect from Fig. 1 (c,d).

For simplicity and in accordance with what we observe from Fig. B1, we will neglect the asymmetric terms from this point onwards. In that case, equation (B.1) is simplified to

$$-\frac{\langle \partial_x m_z \rangle}{\langle m_{\text{ip}}^2 \rangle} \frac{1+\alpha^2}{\gamma_0} v(\mathbf{H}_{\text{ext}}) = \left[H_{\text{ext},x} \frac{\langle m_y \rangle}{\langle m_{\text{ip}}^2 \rangle} - H_{\text{ext},y} \frac{\langle m_x \rangle}{\langle m_{\text{ip}}^2 \rangle} + \alpha H_{\text{ext},z} \right] + M_{\text{s}} (N_{\text{eff},y} - N_{\text{eff},x}) \frac{\langle m_x \rangle \langle m_y \rangle}{\langle m_{\text{ip}}^2 \rangle \zeta_{\text{ms}}}$$

$$+\frac{2D_{\mathrm{DMI}}}{\mu_0 M_{\mathrm{s}}}\left[\frac{\langle\partial_x m_z\rangle\langle m_y\rangle}{\langle m_{\mathrm{ip}}^2\rangle\zeta_{\mathrm{DMI}}}-\frac{\langle\partial_y m_z\rangle\langle m_x\rangle}{\langle m_{\mathrm{ip}}^2\rangle\zeta_{\mathrm{DMI}}}\right]$$
$$+\frac{2A}{\mu_0 M_{\mathrm{s}}}\left[\frac{\langle\partial_{xx} m_x\rangle\langle m_y\rangle}{\langle m_{\mathrm{ip}}^2\rangle\zeta_{\mathrm{exch}}}-\frac{\langle\partial_{yy} m_y\rangle\langle m_x\rangle}{\langle m_{\mathrm{ip}}^2\rangle\zeta_{\mathrm{exch}}}\right] \tag{B.5}$$

References

[1] Robert L Stamps, Stephan Breitkreutz, Johan kerman, Andrii V Chumak, YoshiChika Otani, Gerrit E W Bauer, Jan-Ulrich Thiele, Martin Bowen, Sara A Majetich, Mathias Kläui, Ioan Lucian Prejbeanu, Bernard Dieny, Nora M Dempsey, and Burkard Hillebrands. The 2014 magnetism roadmap. *Journal of Physics D: Applied Physics*, 47(33):333001, 2014.

[2] D. A. Allwood, G. Xiong, C. C. Faulkner, D. Atkinson, D. Petit, and R. P. Cowburn. Magnetic domain-wall logic. *Science*, 309(5741):1688–1692, 2005.

[3] Stuart P. Parkin, Masamitsu Hayashi, and Luc Thomas. Magnetic domain-wall racetrack memory. *Science*, 320(5873):190–194, 2008.

[4] June-Seo Kim, Mohamad-Assaad Mawass, André Bisig, Benjamin Krüger, Robert M Reeve, Tomek Schulz, Felix Büttner, Jungbum Yoon, Chun-Yeol You, Markus Weigand, et al. Synchronous precessional motion of multiple domain walls in a ferromagnetic nanowire by perpendicular field pulses. *Nature communications*, 5, 2014.

[5] Stuart Parkin and See-Hun Yang. Memory on the racetrack. *Nature nanotechnology*, 10(3):195–198, 2015.

[6] K. A. Omari and T. J. Hayward. Chirality-based vortex domain-wall logic gates. *Phys. Rev. Applied*, 2:044001, Oct 2014.

[7] J Vandermeulen, B Van de Wiele, L Dupré, and B Van Waeyenberge. Logic and memory concepts for all-magnetic computing based on transverse domain walls. *Journal of Physics D: Applied Physics*, 48(27):275003, 2015.

[8] I Dzyaloshinskii. On the magnetic structure of the fluorides of transition metals. *Zhur. Eksptl'. i Teoret. Fiz.*, 33, 1957.

[9] Tôru Moriya. Anisotropic superexchange interaction and weak ferromagnetism. *Physical Review*, 120(1):91, 1960.

[10] André Thiaville, Stanislas Rohart, Émilie Jué, Vincent Cros, and Albert Fert. Dynamics of dzyaloshinskii domain walls in ultrathin magnetic films. *EPL (Europhysics Letters)*, 100(5):57002, 2012.

[11] O. Boulle, S. Rohart, L. D. Buda-Prejbeanu, E. Jué, I. M. Miron, S. Pizzini, J. Vogel, G. Gaudin, and A. Thiaville. Domain wall tilting in the presence of the dzyaloshinskii-moriya interaction in out-of-plane magnetized magnetic nanotracks. *Phys. Rev. Lett.*, 111:217203, Nov 2013.

[12] Kwang-Su Ryu, Luc Thomas, See-Hun Yang, and Stuart Parkin. Chiral spin torque at magnetic domain walls. *Nat Nano*, 8(7):527–533, July 2013.

[13] Satoru Emori, Uwe Bauer, Sung-Min Ahn, Eduardo Martinez, and Geoffrey SD Beach. Current-driven dynamics of chiral ferromagnetic domain walls. *Nature materials*, 12(7):611–616, 2013.

[14] Eduardo Martinez, Satoru Emori, and Geoffrey SD Beach. Current-driven domain wall motion along high perpendicular anisotropy multilayers: The role of the rashba field, the spin hall effect, and the dzyaloshinskii-moriya interaction. *Applied Physics Letters*, 103(7):072406, 2013.

[15] Eduardo Martinez, Satoru Emori, Noel Perez, Luis Torres, and Geoffrey SD Beach. Current-driven dynamics of dzyaloshinskii domain walls in the presence of in-plane fields: Full micromagnetic and one-dimensional analysis. *Journal of Applied Physics*, 115(21):213909, 2014.

[16] Satoru Emori, Eduardo Martinez, Kyung-Jin Lee, Hyun-Woo Lee, Uwe Bauer, Sung-Min Ahn, Parnika Agrawal, David C. Bono, and Geoffrey S. D. Beach. Spin hall torque magnetometry of dzyaloshinskii domain walls. *Phys. Rev. B*, 90:184427, Nov 2014.

[17] Yoko Yoshimura, Kab-Jin Kim, Takuya Taniguchi, Takayuki Tono, Kohei Ueda, Ryo Hiramatsu, Takahiro Moriyama, Keisuke Yamada, Yoshinobu Nakatani, and Teruo Ono. Soliton-like magnetic domain wall motion induced by the interfacial dzyaloshinskii-moriya interaction. *Nature Physics*, 2015.

[18] JC Slonczewski. Dynamics of magnetic domain walls. In *MAGNETISM AND MAGNETIC MATERIALS1971 Parts 1 and 2*, volume 5, pages 170–174. AIP Publishing, 1972.

[19] A. Thiaville, J. M. Garca, and J. Miltat. Domain wall dynamics in nanowires. *J. Magn. Magn. Mat.*, 242-245(Part 2):1061–1063, 2002.

[20] A. Thiaville and Y. Nakatani. *Spin Dynamics in Confined Magnetic Structures III*, volume Volume 101/2006 of *Topics Appl. Phys.*, chapter Domain-Wall Dynamics in Nanowires and Nanostrips, pages 161–205. Springer, Berlin–Heidelberg, 2006.

[21] O. A. Tretiakov, D. Clarke, Gia-Wei Chern, Ya. B. Bazaliy, and O. Tchernyshyov. Dynamics of domain walls in magnetic nanostrips. *Phys. Rev. Lett.*, 100:127204, Mar 2008.

[22] D. J. Clarke, O. A. Tretiakov, G.-W. Chern, Ya. B. Bazaliy, and O. Tchernyshyov. Dynamics of a vortex domain wall in a magnetic nanostrip: Application of the collective-coordinate approach. *Phys. Rev. B*, 78:134412, Oct 2008.

[23] J Vandermeulen, B Van de Wiele, A Vansteenkiste, B Van Waeyenberge, and L Dupré. A collective coordinate approach to describe magnetic domain wall dynamics applied to nanowires with high perpendicular anisotropy. *Journal of Physics D: Applied Physics*, 48(3):035001, 2015.

[24] J. Leliaert, B. Van de Wiele, J. Vandermeulen, A. Coene, A. Vansteenkiste, L. Laurson, G. Durin, B. Van Waeyenberge, and L. Dupré. Thermal effects on transverse domain wall dynamics in magnetic nanowires. *Applied Physics Letters*, 106(20):–, 2015.

[25] Jonathan Leliaert, Ben Van de Wiele, Arne Vansteenkiste, Lasse Laurson, Gianfranco Durin, Luc Dupré, and Bartel Van Waeyenberge. Creep turns linear in narrow ferromagnetic nanostrips. *Scientific Reports*, 6:20472, 2016.

[26] T.L. Gilbert. A phenomenological theory of damping in ferromagnetic materials. *Magnetics, IEEE Transactions on*, 40(6):3443–3449, Nov 2004.

[27] D. G. Porter and M. J. Donahue. Velocity of transverse domain wall motion along thin, narrow strips. *J. Appl. Phys.*, 95(11):6729–6731, 2004.

[28] Anders Smith, Kaspar Kirstein Nielsen, DV Christensen, Christian Robert Haffenden Bahl, Rasmus Bjørk, and J Hattel. The demagnetizing field of a nonuniform rectangular prism. *Journal of Applied Physics*, 107(10):103910, 2010.

[29] A. Mougin, M. Cormier, J. P. Adam, P. J. Metaxas, and J. Ferré. Domain wall mobility, stability and walker breakdown in magnetic nanowires. *Europhysics Letters (EPL)*, 78(5):57007, 2007.

[30] N. L. Schryer and L. R. Walker. The motion of 180^o domain walls in uniform dc magnetic fields. *J. Appl. Phys.*, 45(12):5406–5421, 1974.

[31] Arne Vansteenkiste, Jonathan Leliaert, Mykola Dvornik, Mathias Helsen, Felipe Garcia-Sanchez, and Bartel Van Waeyenberge. The design and verification of mumax3. *AIP Advances*, 4(10):–, 2014.

[32] Eduardo Martinez. The stochastic nature of the domain wall motion along high perpendicular anisotropy strips with surface roughness. *J. Phys.: Condens. Matter*, 24(2):024206, 2012.